Anomalous Hall effect at a PtOx/Co interface

Hiroki Hayashi,[1] Akio Asami,[1] and Kazuya Ando[1,2,*]

[1]*Department of Applied Physics and Physico-Informatics, Keio University, Yokohama 223-8522, Japan*
[2]*Center for Spintronics Research Network (CSRN), Keio University, Yokohama 223-8522, Japan*

We study the anomalous Hall effect at a PtOx/Co interface. We extracted the intrinsic and extrinsic contributions to the anomalous Hall effect in SiO$_2$/Co/SiO$_2$ and PtOx/Co/SiO$_2$ films by measuring temperature dependence of the anomalous Hall resistivity. The result shows that the intrinsic anomalous Hall effect in the PtOx/Co/SiO$_2$ film is almost identical to that in the SiO$_2$/Co/SiO$_2$ film. In contrast, the extrinsic anomalous Hall effect is clearly different between the SiO$_2$/Co/SiO$_2$ and PtOx/Co/SiO$_2$ films. The anomalous Hall effect for various Co-layer thicknesses t at various temperatures reveals that the extrinsic anomalous Hall resistivity shows a t^{-1} dependence in the PtOx/Co/SiO$_2$ film, while it is almost independent of t in the SiO$_2$/Co/SiO$_2$ film. This result demonstrates the extrinsic anomalous Hall effect originating from the PtOx/Co interface. Our results show that both the side-jump and skew-scattering mechanisms contribute to the interfacial anomalous Hall effect, which can be attributed to the formation of Co-O bonds and electron scattering by Pt impurities at the PtOx/Co interface.

I. INTRODUCTION

Over the decades, the family of Hall effects has offered an attractive field of research in condensed-matter physics [1–4]. The study of the unconventional Hall effects began with the discovery of the anomalous Hall effect (AHE), which appears in solids with broken time-reversal symmetry as a consequence of spin-orbit coupling (SOC). Although the AHE was discovered in a ferromagnetic metal more than a century ago, it still attracts considerable experimental and theoretical interest.

The AHE in ferromagnetic metals arises from intrinsic and extrinsic mechanisms. The intrinsic AHE is induced by the Berry curvature, which depends on the band structure [5]. The extrinsic AHE, including the skew scattering and side-jump mechanisms, originates from spin-dependent scattering on structural defects or impurities with strong SOC [6,7]. The mechanism of the AHE has been studied experimentally based on the power-law dependence of the anomalous Hall (AH) resistivity ρ_{xy} on the longitudinal resistivity ρ_{xx}; $\rho_{xy} \propto \rho_{xx}^2$ is expected for the intrinsic and side-jump mechanisms, while $\rho_{xy} \propto \rho_{xx}$ is expected for the skew-scattering mechanism [8–12]. The predominant mechanism of the AHE is determined by the longitudinal resistivity [2].

The AHE has been observed to be modified when a ferromagnetic metal is interfaced with nonmagnetic materials. The AHE in metallic multilayers, such as Fe/Ta, Fe/Au, Ni/Au, Co/Pd, and Co/Pt, suggests that spin-dependent scattering at interfaces, as well as the bulk of a ferromagnetic metal, plays a key role in the AHE in heterostructures [13–17]. Previous studies have also demonstrated that oxygen distribution and their chemical bonds affect the interfacial contribution to the AHE in ferromagnetic-metal/oxide heterostructures [18–20].

The interfacial contributions to spin-dependent transport is also essential in recent progress in spin orbitronics, a branch of spintronics that aims at discovering phenomena and functionalities originating from the SOC [21–26]. The foundation of spin orbitronics is the conversion between charge and spin thorough the bulk or interface SOC. The interface SOC plays a major role in the charge-spin conversion in metal-oxide/ferromagnetic-metal heterostrutures, where the spin Hall effect of the nonmagnetic layer attached to the ferromagnetic metal can be neglected [27,28]. Recent studies have revealed that heavy-metal oxides, such as PtOx, enables highly efficient charge-spin conversion in the metal-oxide/ferromagnetic-metal structure [29–31]. These results indicate that the exploration of the spin-dependent transport at the heavy-metal-oxide/ferromagnetic-metal interface is crucial for the fundamental understanding and practical application of the spin-orbitronic devices.

In this paper, we investigate the AHE at the PtOx/Co interface. By measuring temperature dependence of the AHE, we extracted the intrinsic and extrinsic contributions to the AHE. We found that the extrinsic AHE in a PtOx/Co/SiO$_2$ film is strongly enhanced by decreasing the Co-layer-thickness, while this enhancement disappears when the PtOx is replaced with SiO$_2$. The enhanced AHE can be attributed to the sizable side-jump and skew scattering AHE at the PtOx/Co interface due to the formation of Co-O bonds and electron scattering by Pt impurities.

II. EXPERIMENTAL METHOD

The samples used in this study are SiO$_2$(10)/Co(t)/SiO$_2$-cap(4) and PtOx(4)/Co(t)/SiO$_2$-cap(4) films [see Fig. 1(a)], where the numbers in parentheses represent the thickness in
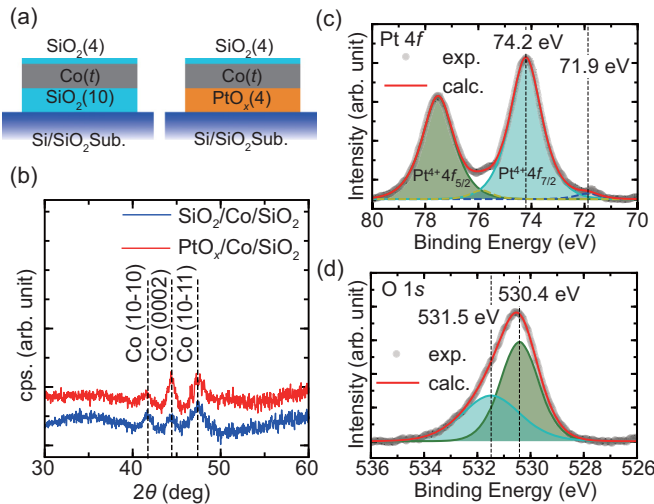
*ando@appi.keio.ac.jp

FIG. 1. (a) The schematic illustration of the $SiO_2/Co/SiO_2$ and $PtO_x/Co/SiO_2$ films. The numbers in parentheses represent the thickness in units of nm. The Co-layer thickness t was varied from 10 to 100 nm. (b) XRD profiles of the 100-nm-thick Co film fabricated on the SiO_2 and PtO_x layers. The red and blue curves are the data for the $SiO_2/Co/SiO_2$ and $PtO_x/Co/SiO_2$ films, respectively. The black dashed lines represent 41.7°, 44.4°, and 47.4°. (c), (d) The XPS spectra for the PtO_x film, where (c) Pt $4f$ and (d) O $1s$. The solid circles in gray are the experimental data. The solid circles in red are the fitting result. To eliminate the charge effect on the film surface, all of the XPS spectra have been corrected by using the binding energy of C $1s$ (284.0 eV).

units of nm. The films were sputtered on thermally oxidized Si/SiO$_2$(100) substrates at room temperature, where the base pressure was better than 3.0×10^{-5} Pa. First, for the fabrication of the $SiO_2/Co/SiO_2$ ($PtO_x/Co/SiO_2$) film, the SiO$_2$ (PtO$_x$) layer was deposited by radio frequency magnetron sputtering in an argon (oxygen) atmosphere, where the working pressure was 0.24 (1.75) Pa and the deposition rate was 0.2 (0.1) Å/s. Then, the Co layer was deposited in an argon atmosphere by direct current magnetron sputtering at 1.52 Pa with the deposition rate of 0.9 Å/s. For the fabrication of the $PtO_x/Co/SiO_2$ film, the chamber was evacuated to 3.0×10^{-5} Pa after the PtO$_x$ deposition to prevent the oxidation of the Co layer during the Co deposition. The Co thickness t was changed from 10 to 100 nm. Finally, a 4-nm-thick SiO$_2$ capping layer was deposited on the Co layer to avoid natural oxidation of the films.

To study the AHE, the $SiO_2/Co/SiO_2$ and $PtO_x/Co/SiO_2$ films were pattered into Hall bars with the width of 4 μm and length of 40 μm using negative photolithography and liftoff technique. We measured the longitudinal resistivity ρ_{xx} and Hall resistivity ρ_{xy} for the $SiO_2/Co/SiO_2$ and $PtO_x/Co/SiO_2$ films using Physical Property Measurements Systems (Quantum Design PPMS-14 T system). For the transport measurement, we used the standard lock-in technique, where an alternating current with a frequency of 17 Hz and an amplitude of 1 mA were applied. In both films, we assume that the applied current flows only in the Co layer; we neglect the current flow in the PtO$_x$ layer because the resistivity of

the PtO$_x$ layer (larger than 2.2×10^7 $\mu\Omega$ cm) is more than five orders of magnitude larger than that of the Co layer (around 100 $\mu\Omega$ cm). In the present paper, all the error bars are the fitting errors, i.e., within the sample (between analysis) variance [32].

To investigate the microstructure of the Co film on the SiO$_2$ and PtO$_x$ layers, x-ray diffraction (XRD) was measured with a Bruker D8 Discover diffractometer in the rocking curve mode with a two dimensional detector using a Cu-Kα radiation ($\lambda = 1.54$ Å). For the PtO$_x$ film, the chemical profile was investigated using x-ray photoelectron spectroscopy (XPS, JPS-9010TR) with a Mg-Kα radiation ($h\nu = 1253.6$ eV) and a hemispherical energy analyzer (pass energy of 10 eV with a resolution of 0.03 eV) to probe the surface of the samples.

III. RESULTS AND DISCUSSION

We show the XRD spectra measured for $SiO_2(10)/Co(100)/SiO_2$ and $PtO_x(4)/Co(100)/SiO_2$ films in Fig. 1(b). As shown in Fig. 1(b), hcp-Co(10-10), hcp-Co(0002) or fcc-Co(111), and hcp-Co(10-11) peaks were observed for the Co films deposited on the SiO$_2$ and PtO$_x$ layers [33,34]. This result indicates that the XRD pattern is almost independent of the seed layer, showing similar polycrystalline nature of the Co layers deposited on the SiO$_2$ and PtO$_x$ layers. We also measured the XRD for a PtO$_x$ film with the thickness of 45 nm and found that no peak can be observed.

For the PtO$_x$ film, we measured the XPS as shown in Figs. 1(c) and 1(d). As shown in Fig. 1(c), we observed peaks at the binding energy of 71.2, 72.3, and 74.0 eV, which correspond to the chemical state of Pt^0, Pt^{2+}, and Pt^{4+}($J = 7/2$), respectively [35]. This result shows that the PtO$_x$ film fabricated by the reactive sputtering is predominated by PtO$_2$. This is supported by the fact that, in the PtO$_x$ film, the O $1s$ peak is around 530.2 eV [Fig. 1(d)] [35].

Figure 2(a) shows the Hall resistance R_{xy} for the $PtO_x/Co(15)/SiO_2$ film as a function of the magnetic field $\mu_0 H$, applied perpendicular to the film [see also Fig. 2(b)]. We determined the AH resistivity ρ_{xy} using $\rho_{xy} = t/2(R_{xy}^+ - R_{xy}^-)$ at various temperatures T, where R_{xy}^+ and R_{xy}^- were obtained from the Hall resistance at high positive and negative magnetic fields [see the dashed lines in Fig. 2(a)]. In Fig. 2(b), we show the AH resistivity as a function of the Co-layer thickness. This result shows that the AH resistivity increases with decreasing the thickness in both $PtO_x/Co/SiO_2$ and $SiO_2/Co/SiO_2$ films. The enhancement of the AH resistivity with decreasing the thickness in the $SiO_2/Co/SiO_2$ film shows a non-negligible AHE originating at the SiO$_2$/Co interface, which is consistent with a previous report [36]. We note that the enhancement of the AH resistivity in the $PtO_x/Co/SiO_2$ film is more significant than that in the $SiO_2/Co/SiO_2$ film. This indicates a stronger interfacial AHE originating at the PtO$_x$/Co interface.

In Figs. 2(c) and 2(d), we show the temperature T dependence of the AH resistivity ρ_{xy} for the $PtO_x/Co(15)/SiO_2$ and $SiO_2/Co(15)/SiO_2$ films. We also show the temperature T dependence of the longitudinal resistivity ρ_{xx} in Figs. 2(c) and 2(d). This result shows that the T dependence of ρ_{xx} is well
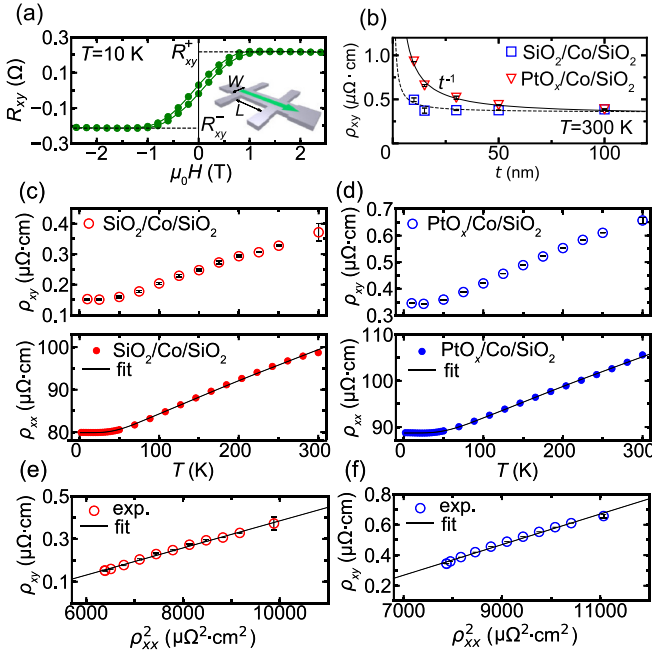
FIG. 2. (a) The perpendicular magnetic field $\mu_0 H$ dependence of the Hall resistance R_{xy} for the PtO$_x$/Co(15)/SiO$_2$ film at 10 K. $R_{xy}^{+(-)}$ represents extrapolated values obtained by fitting R_{xy} using a linear function at the positive (negative) high magnetic field. The inset shows schematic illustration of the Hall bar with the width $W = 4$ μm and length $L = 40$ μm. (b) The Co-thickness t dependence of AH resistivity ρ_{xy} for SiO$_2$/Co/SiO$_2$ film (open squares in blue) and PtO$_x$/Co/SiO$_2$ film (open triangles in red) at 300 K. (c), (d) The temperature T dependence of the longitudinal resistivity ρ_{xx} and AH resistivity ρ_{xy} for the SiO$_2$/Co(15)/SiO$_2$ and PtO$_x$/Co(15)/SiO$_2$ films. The black curve is the fitting results using Eq. (1). (e), (f) The AH resistivity ρ_{xy} as a function of the square of the longitudinal resistivity ρ_{xx}^2 for the SiO$_2$/Co(15)/SiO$_2$ and PtO$_x$/Co(15)/SiO$_2$ films. The black lines are the fitting result using Eq. (2).

reproduced by the Bloch-Grüneisen formula [37,38],

$$\rho_{xx}(T) = \rho_{xx,0} + A\left(\frac{T}{T_D}\right)^5 \int_0^{T_D/T} \frac{x^5}{(e^x - 1)(1 - e^{-x})}dx,$$

(1)

where $\rho_{xx,0}$ is the residual resistivity, A characterizes electron-phonon scattering, and T_D is the Debye temperature. Using the result shown in Figs. 2(c) and 2(d), we plot ρ_{xy} as a function of ρ_{xx}^2 for the PtO$_x$/Co(15)/SiO$_2$ and SiO$_2$/Co(15)/SiO$_2$ films in Figs. 2(e) and 2(f). This result is consistent with the empirical relation of the AH resistivity ρ_{xy},

$$\rho_{xy} = \sigma_{int}\rho_{xx}^2 + \alpha_{ss}\rho_{xx,0} + \sigma_{sj}\rho_{xx,0}^2,$$

(2)

where σ_{int} is the intrinsic AH conductivity, α_{ss} is the skew scattering angle, and σ_{sj} is the side-jump AH conductivity [9,10,39,40]. In the present paper, we neglect the skew scattering induced by phonons, reported previously [10]. Using Eq. (2), we analyzed the ρ_{xx}^2 dependence of ρ_{xy} for the PtO$_x$/Co(t)/SiO$_2$ and SiO$_2$/Co(t)/SiO$_2$ films with various t. By changing t, the residual resistivity $\rho_{xx,0}$ changes as shown in Fig. 3(a). This result shows that $\rho_{xx,0}$ shows a t^{-1}
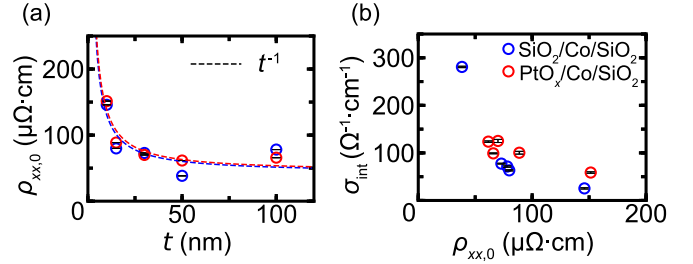

FIG. 3. (a) The Co-layer thickness t dependence of residual resistivity $\rho_{xx,0}$ for the SiO$_2$/Co/SiO$_2$ film (open circles in blue) and PtO$_x$/Co/SiO$_2$ film (open circles in red). The dashed curves are the fitting result using a function proportional to t^{-1}. The error bars represent the standard deviation. The deviation of the data from the t^{-1} dependence arises from the between sample variance. (b) The residual resistivity $\rho_{xx,0}$ dependence of intrinsic AHE conductance σ_{int} for the SiO$_2$/Co/SiO$_2$ film (open circles in blue) and PtO$_x$/Co/SiO$_2$ film (open circles in red), obtained from Eq. (2).

dependence, consistent with the Mayadas and Shatzkes model [41] in both PtO$_x$/Co/SiO$_2$ and SiO$_2$/Co/SiO$_2$ films.

By fitting the measured ρ_{xx}^2 dependence of ρ_{xy} using Eq. (2), we extracted σ_{int} for the PtO$_x$/Co/SiO$_2$ and SiO$_2$/Co/SiO$_2$ films with various t. We plot the extracted values of σ_{int} with respect to $\rho_{xx,0}$ in Fig. 3(b), where we used the t dependence of $\rho_{xx,0}$ shown in Fig. 3(a). Figure 3(b) indicates that the intrinsic AH conductivity σ_{int} decreases monotonically with the residual resistivity $\rho_{xx,0}$ in both PtO$_x$/Co/SiO$_2$ and SiO$_2$/Co/SiO$_2$ films. This result is consistent with a previous calculation based on the tight-binding model [11]. Figure 3(b) also shows that the intrinsic contribution to the AHE is comparable between the PtO$_x$/Co/SiO$_2$ and SiO$_2$/Co/SiO$_2$ films. This is reasonable because of the similar bulk crystallinity of the Co layer in the PtO$_x$/Co/SiO$_2$ and SiO$_2$/Co/SiO$_2$ films, confirmed by the XRD measurement. The decrease of σ_{int} with $\rho_{xx,0}$ is consistent with the AHE in the dirty limit [11,39].

In contrast to the intrinsic contribution, the extrinsic contribution to the AHE,

$$\rho_{ext} = \alpha_{ss}\rho_{xx,0} + \sigma_{sj}\rho_{xx,0}^2,$$

(3)

is clearly different between the PtO$_x$/Co/SiO$_2$ and SiO$_2$/Co/SiO$_2$ films. In Fig. 4(a), we show t dependence of the absolute value of the extrinsic AH resistivity $|\rho_{ext}|$ extracted from the fitting using Eq. (2). When $t = 100$ nm, $|\rho_{ext}|$ is comparable between the PtO$_x$/Co/SiO$_2$ and SiO$_2$/Co/SiO$_2$ films as shown in Fig. 4(a). This is consistent with the fact that the interface contribution to the AHE is negligible in the thick-film limit. In the SiO$_2$/Co/SiO$_2$ film, $|\rho_{ext}|$ is unchanged by decreasing the Co thickness from $t = 100$ nm, where the bulk contribution dominates the AHE. This result indicates that the AHE in the SiO$_2$/Co/SiO$_2$ film is dominated by the bulk contribution, and the contribution from the SiO$_2$/Co interface is negligible. In contrast to the almost t-independent $|\rho_{ext}|$ in the SiO$_2$/Co/SiO$_2$ film, $|\rho_{ext}|$ shows a t^{-1} dependence in the PtO$_x$/Co/SiO$_2$ film [see the red dotted line in Fig. 4(a)]. By decreasing t, $|\rho_{ext}|$ of the PtO$_x$/Co/SiO$_2$ film becomes 2.5 times larger than that of the SiO$_2$/Co/SiO$_2$ film, indicating that the AHE in the thin
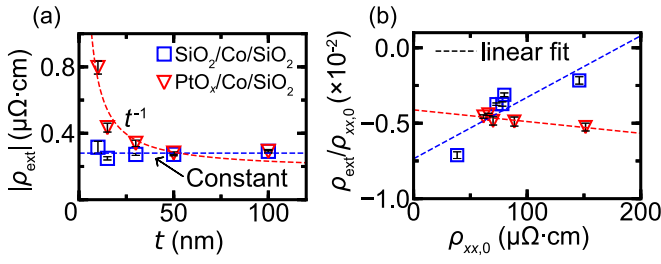
FIG. 4. (a) The Co-layer thickness t dependence of the absolute value of the extrinsic AHE resistivity $|\rho_{ext}|$ for the $SiO_2/Co/SiO_2$ film (open squares in blue) and $PtO_x/Co/SiO_2$ film (open triangles in red). The dashed lines represent t^{-1} and constant. (b) The residual resistivity $\rho_{xx,0}$ dependence of $\rho_{ext}/\rho_{xx,0}$ for the $SiO_2/Co/SiO_2$ film (open squares in blue) and $PtO_x/Co/SiO_2$ film (open triangles in red). The dashed lines represent the fitting result using Eq. (3).

$PtO_x/Co/SiO_2$ film is dominated by the contribution from the extrinsic scattering at the PtO_x/Co interface.

To reveal the side-jump and skew-scattering contributions to the AHE in the $PtO_x/Co/SiO_2$ film, we plot $\rho_{ext}/\rho_{xx,0}$ dependence of $\rho_{xx,0}$ in Fig. 4(b). Figure 4(b) shows that $\rho_{ext}/\rho_{xx,0}$ changes linearly with $\rho_{xx,0}$ in the $PtO_x/Co/SiO_2$ and $SiO_2/Co/SiO_2$ films. This result indicates that the sign of the slope is opposite between the $PtO_x/Co/SiO_2$ and $SiO_2/Co/SiO_2$ films. Here, the linear relation between $\rho_{ext}/\rho_{xx,0}$ and $\rho_{xx,0}$ allows us to determine the skew scattering angle α_{ss} and side-jump AH conductivity σ_{sj} because of Eq. (3). Equation (3) predicts that the intercept and slope correspond to the skew-scattering angle α_{ss} and side-jump AH conductivity σ_{sj}, respectively. For the $SiO_2/Co/SiO_2$ film, we obtained $\alpha_{ss}^{SiO_2/Co/SiO_2} = -0.75 \pm 0.14\%$ and $\sigma_{sj}^{SiO_2/Co/SiO_2} = 42.3 \pm 15.8~\Omega^{-1}~cm^{-1}$. These values are consistent with a previous report [9,39]. For the $PtO_x/Co/SiO_2$ film, we obtained $\alpha_{ss}^{PtO_x/Co/SiO_2} = -0.40 \pm 0.02\%$ and $\sigma_{sj}^{PtO_x/Co/SiO_2} = -8.34 \pm 2.55~\Omega^{-1}~cm^{-1}$. Because of the weak contribution from the SiO_2/Co interface to the AHE, the difference in α_{ss} and σ_{sj} can be approximately attributed to the AHE due to the PtO_x/Co interface.

Since the contribution from the SiO_2/Co interface to the AHE is negligible, the interfacial skew-scattering angle $\Delta\alpha_{ss}^{PtO_x/Co}$ and side-jump conductivity $\Delta\sigma_{sj}^{PtO_x/Co}$ due to the PtO_x/Co interface can be obtained as $\Delta\alpha_{ss}^{PtO_x/Co} = \alpha_{ss}^{PtO_x/Co/SiO_2} - \alpha_{ss}^{SiO_2/Co/SiO_2} = 0.35 \pm 0.14\%$ and $\Delta\sigma_{sj}^{PtO_x/Co} = \sigma_{sj}^{PtO_x/Co/SiO_2} - \sigma_{sj}^{SiO_2/Co/SiO_2} = -50.6 \pm 16.0~\Omega^{-1}~cm^{-1}$. Since $\alpha_{ss}^{SiO_2/Co/SiO_2} < 0$ and $\sigma_{sj}^{SiO_2/Co/SiO_2} > 0$, this result demonstrates the opposite sign of the interfacial skew scattering and side-jump AHE between the Co bulk and PtO_x/Co interface.

The interface AHE in the $PtO_x/Co/SiO_2$ film can be attributed to the formation of Co-O bonds and electron scattering by Pt impurities at the PtO_x/Co interface. The extrinsic AHE in heterostructures is highly sensitive to the interfacial oxygen distribution [19]. In the $PtO_x/Co/SiO_2$ film, according to the Ellingham diagram, the standard Gibbs free energy ΔG^0 of Pt is larger than that of Co, whereas ΔG^0 of Si is smaller than that of Co [42,43]: $\Delta G_{PtO_2}^0(Pt \to PtO_2) > \Delta G_{CoO}^0(Co \to CoO) > \Delta G_{SiO_2}^0(Si \to SiO_2)$. This suggests
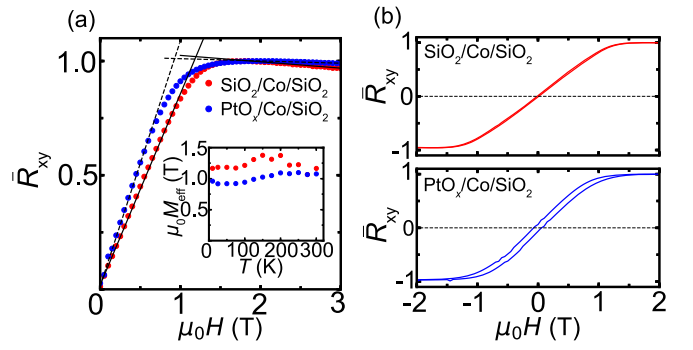

FIG. 5. (a) The Hall resistance $\bar{R}_{xy} = R_{xy}/R_{xy}^{max}$ as a function of the perpendicular magnetic field μ_0H for the $PtO_x/Co(10)/SiO_2$ and $SiO_2/Co(10)/SiO_2$ films at $T = 10$ K. R_{xy}^{max} is the maximum value of R_{xy}. The inset shows temperature T dependence of the effective demagnetization field μ_0M_{eff} for the $SiO_2/Co/SiO_2$ and $PtO_x/Co/SiO_2$ films. (b) $\bar{R}_{xy}$ as a function of μ_0H at $T = 10$ K for the $SiO_2/Co/SiO_2$ and $PtO_x/Co/SiO_2$ films.

that when Co is attached to PtO_x, Co oxidation and PtO_x reduction at the interface are expected, while at the SiO_2/Co interface, the oxidation of Co should be minor, compared to the PtO_x/Co interface. The Co-O bonds formed in PtO_x/Co interface can give rise to the side-jump contribution to the interface AHE [17,19]. We also note that the skew scattering can be enhanced by impurity scattering due to heavy elements [44–46]. Because of the strong SOC of Pt, compared to that of Si, the AHE is expected to be enhanced by replacing SiO_2 with PtO_x.

The interfacial oxygen distribution and their chemical bonds are known to influence the perpendicular magnetic anisotropy (PMA). To characterize the PMA at the PtO_x/Co interface, we analyzed the effective demagnetization field M_{eff} using the AHE result. Figure 5(a) shows the Hall resistance $\bar{R}_{xy} = R_{xy}/R_{xy}^{max}$ as a function of the perpendicular magnetic field μ_0H for the $PtO_x/Co(10)/SiO_2$ and $SiO_2/Co(10)/SiO_2$ films, where R_{xy}^{max} is the maximum value of R_{xy}. In Fig. 5(a), the ordinary Hall effect (OHE) contribution to $\bar{R}_{xy}$ was determined by fitting the slope at high magnetic fields, beyond magnetic saturation, while the AHE contribution was determined at low magnetic field by extrapolating the slope at $\mu_0H = 0$. From the coincidence point of the linear fits for the OHE and AHE, we obtained the effective demagnetization field μ_0M_{eff} for the $PtO_x/Co(10)/SiO_2$ and $SiO_2/Co(10)/SiO_2$ films at various temperatures T [see the inset to Fig. 5(a)]. This result shows that μ_0M_{eff} of the $PtO_x/Co/SiO_2$ film is smaller than that of the $SiO_2/Co/SiO_2$ film, showing that the effective interfacial PMA energy at the PtO_x/Co interface is larger than that at the SiO_2/Co interface. The larger K_s at the PtO_x/Co interface is supported by the larger coercivity in the $PtO_x/Co/SiO_2$ film, compared to that in the $SiO_2/Co/SiO_2$ film [see Fig. 5(b)]. The increase of K_s due to the replacement of SiO_2 with PtO_x is consistent with the formation of the interfacial Co-O bonds [47]. Using $\mu_0M_{eff} = \mu_0M_s - 2K_s/M_s t$ [48], we obtained the difference in the effective interfacial PMA energy between the PtO_x/Co and SiO_2/Co interfaces as $K_s^{PtO_x/Co} - K_s^{SiO_2/Co} = 0.7 \sim 1.5$ mJ/m^2, where M_s is saturation magnetization and

$K_s^{\text{PtO}_x(\text{SiO}_2)/\text{Co}}$ is the effective interfacial PMA energy at the PtO$_x$(SiO$_2$)/Co interface.

IV. CONCLUSION

In summary, we have investigated the AHE in the SiO$_2$/Co/SiO$_2$ and PtO$_x$/Co/SiO$_2$ films to reveal the AHE at the PtO$_x$/Co interface. By measuring the thickness and temperature dependence of the AHE, we extracted the intrinsic and extrinsic contributions to the AHE. The result shows that the intrinsic AHE in the PtO$_x$/Co/SiO$_2$ film is comparable to that in the SiO$_2$/Co/SiO$_2$ film. In contrast, the extrinsic AHE is clearly different between the SiO$_2$/Co/SiO$_2$ and PtO$_x$/Co/SiO$_2$ films. When the Co layer is thicker than 30 nm, the extrinsic AHE in the PtO$_x$/Co/SiO$_2$ film is comparable to that in the SiO$_2$/Co/SiO$_2$ film. However, the extrinsic AHE is strongly enhanced in the PtO$_x$/Co/SiO$_2$ film by decreasing the thickness. Our results show that the enhancement of the AHE originates from the sizable extrinsic AHE due to the skew and side-jump mechanism at the PtO$_x$/Co interface. The enhanced AHE at the PtO$_x$/Co interface can be attributed to the formation of Co-O bonds and electron scattering by Pt impurities at the PtO$_x$/Co interface. Recent studies have reported efficient generation of the spin-orbit torques in ferromagnetic-metal/metal-oxide heterostructures. Although the origin of the torques is largely attributed to the ferromagnetic-metal/metal-oxide interface, the underlying mechanisms are still unclear. Our finding of the sizable extrinsic AHE originating at the PtO$_x$/Co interface suggests that the spin-dependent extrinsic scattering at the interface may contribute to the efficient spin-torque generation. Thus, further studies on the relation between the interfacial spin-orbit torque and interfacial AHE by varying the oxidation level will provide an important information for the fundamental understating of the interfacial spin-orbitronics phenomena.

[1] K. von Klitzing, Rev. Mod. Phys. **58**, 519 (1986).

[2] N. Nagaosa, J. Sinova, S. Onoda, A. H. MacDonald, and N. P. Ong, Rev. Mod. Phys. **82**, 1539 (2010).

[3] J. Sinova, S. O. Valenzuela, J. Wunderlich, C. H. Back, and T. Jungwirth, Rev. Mod. Phys. **87**, 1213 (2015).

[4] B. S. Kim, J. Phys.: Condens. Matter **31**, 383001 (2019).

[5] R. Karplus and J. Luttinger, Phys. Rev. **95**, 1154 (1954).

[6] J. Smit, Physica **24**, 39 (1958).

[7] L. Berger, Phys. Rev. B **2**, 4559 (1970).

[8] S. R. Shinde, S. B. Ogale, J. S. Higgins, H. Zheng, A. J. Millis, V. N. Kulkarni, R. Ramesh, R. L. Greene, and T. Venkatesan, Phys. Rev. Lett. **92**, 166601 (2004).

[9] D. Hou, Y. Li, D. Wei, D. Tian, L. Wu, and X. Jin, J. Phys.: Condens. Matter **24**, 482001 (2012).

[10] Y. Tian, L. Ye, and X. Jin, Phys. Rev. Lett. **103**, 087206 (2009).

[11] T. Naito, D. S. Hirashima, and H. Kontani, Phys. Rev. B **81**, 195111 (2010).

[12] D. Hou, G. Su, Y. Tian, X. Jin, S. A. Yang, and Q. Niu, Phys. Rev. Lett. **114**, 217203 (2015).

[13] Q. Zhang, J. Zhang, Y. Zhao, Y. Wen, P. Li, S. Zhang, X. He, J. Zhang, and X. Zhang, AIP Adv. **8**, 055813 (2018).

[14] Q. Zhang, P. Li, Y. Wen, C. Zhao, J. W. Zhang, A. Manchon, W. B. Mi, Y. Peng, and X. X. Zhang, Phys. Rev. B **94**, 024428 (2016).

[15] Q. Zhang, P. Li, Y. Wen, X. He, Y. Zhao, J. Zhang, and X. Zhang, J. Phys. D: Appl. Phys. **50**, 235002 (2017).

[16] Z. B. Guo, W. B. Mi, R. O. Aboljadayel, B. Zhang, Q. Zhang, P. G. Barba, A. Manchon, and X. X. Zhang, Phys. Rev. B **86**, 104433 (2012).

[17] S.-L. Jiang, X. Chen, X.-J. Li, K. Yang, J.-Y. Zhang, G. Yang, Y.-W. Liu, J.-H. Lu, D.-W. Wang, J. Teng, and G.-H. Yu, Appl. Phys. Lett. **107**, 112404 (2015).

[18] S. Zhang, J. Teng, J. Zhang, Y. Liu, J. Li, G. Yu, and S. Wang, Appl. Phys. Lett. **97**, 222504 (2010).

[19] W. Peng, J. Zhang, L. Luo, G. Feng, and G. Yu, J. Appl. Phys. **125**, 093906 (2019).

[20] J. Zhang, W. Peng, G. Yu, Z. He, F. Yang, W. Ji, C. Hu, and S. Wang, ACS Appl. Mater. Interfaces **11**, 24751 (2019).

[21] J. Puebla, F. Auvray, N. Yamaguchi, M. Xu, S. Z. Bisri, Y. Iwasa, F. Ishii, and Y. Otani, Phys. Rev. Lett. **122**, 256401 (2019).

[22] L. Zhu, D. C. Ralph, and R. A. Buhrman, Phys. Rev. Lett. **122**, 077201 (2019).

[23] A. Nomura, T. Tashiro, H. Nakayama, and K. Ando, Appl. Phys. Lett. **106**, 212403 (2015).

[24] H. Nakayama, Y. Kanno, H. An, T. Tashiro, S. Haku, A. Nomura, and K. Ando, Phys. Rev. Lett. **117**, 116602 (2016).

[25] H. Nakayama, T. Yamamoto, H. An, K. Tsuda, Y. Einaga, and K. Ando, Sci. Adv. **4**, eaar3899 (2018).

[26] H. Nakayama, H. An, A. Nomura, Y. Kanno, S. Haku, Y. Kuwahara, H. Sakimura, and K. Ando, Appl. Phys. Lett. **110**, 222406 (2017).

[27] T. Gao, A. Qaiumzadeh, H. An, A. Musha, Y. Kageyama, J. Shi, and K. Ando, Phys. Rev Lett. **121**, 017202 (2018).

[28] A. Asami, H. An, A. Musha, T. Gao, M. Kuroda, and K. Ando, Phys. Rev. B **99**, 024432 (2019).

[29] K.-U. Demasius, T. Phung, W. Zhang, B. P. Hughes, S.-H. Yang, A. Kellock, W. Han, A. Pushp, and S. S. Parkin, Nat. Commun. **7**, 10644 (2016).

[30] H. An, T. Ohno, Y. Kanno, Y. Kageyama, Y. Monnai, H. Maki, J. Shi, and K. Ando, Sci. Adv. **4**, eaar2250 (2018).

[31] H. An, Y. Kanno, A. Asami, and K. Ando, Phys. Rev. B **98**, 014401 (2018).

[32] B. Geelhoed, *Approaches in Material Sampling* (IOS Press, Amsterdam, 2010).

[33] L. Fallarino, O. Hovorka, and A. Berger, Phys. Rev. B **94**, 064408 (2016).

[34] A. Tarka, M. Zybert, Z. Kindler, J. Szmurło, B. Mierzwa, and W. Raróg-Pilecka, Appl. Catal. A: Gen. **532**, 19 (2017).

[35] D. A. Svintsitskiy, L. S. Kibis, A. I. Stadnichenko, S. V. Koscheev, V. I. Zaikovskii, and A. I. Boronin, Chem. Phys. Chem. **16**, 3318 (2015).

[36] R. Hao, J. Su, Q. Huang, T. Zhou, J. Cai, L. Bai, G. Han, S. Yu, G. Liu, S. Yan, and S. Kang, J. Magn. Magn. Mater. **478**, 187 (2019).

[37] G. White, Can. J. Phys. **34**, 1328 (1956).

[38] G. K. White and S. Woods, Philos. Trans. R. Soc. London Ser. A **251**, 273 (1959).

[39] E. Sagasta, J. Borge, L. Esteban, Y. Omori, M. Gradhand, Y. C. Otani, L. E. Hueso, and F. Casanova, Phys. Rev. B **100**, 100407(R) (2019).

[40] G. Su, Y. Li, D. Hou, X. Jin, H. Liu, and S. Wang, Phys. Rev. B **90**, 214410 (2014).

[41] A. F. Mayadas and M. Shatzkes, Phys. Rev. B **1**, 1382 (1970).

[42] J. Jeffes, *Encyclopedia of Materials: Science and Technology* (Elsevier, Oxford, 2001), p. 2751.

[43] J. J. Yang, J. P. Strachan, F. Miao, M.-X. Zhang, M. D. Pickett, W. Yi, D. A. Ohlberg, G. Medeiros-Ribeiro, and R. S. Williams, Appl. Phys. A **102**, 785 (2011).

[44] A. Fert, A. Friederich, and A. Hamzic, J. Magn. Magn. Mater. **24**, 231 (1981).

[45] Y. Niimi, Y. Kawanishi, D. H. Wei, C. Deranlot, H. X. Yang, M. Chshiev, T. Valet, A. Fert, and Y. Otani, Phys. Rev. Lett. **109**, 156602 (2012).

[46] T. Tanaka and H. Kontani, New J. Phys. **11**, 013023 (2009).

[47] A. Manchon, C. Ducruet, L. Lombard, S. Auffret, B. Rodmacq, B. Dieny, S. Pizzini, J. Vogel, V. Uhlíř, M. Hochstrasser *et al.*, J. Appl. Phys. **104**, 043914 (2008).

[48] V. Tshitoyan, C. Ciccarelli, A. P. Mihai, M. Ali, A. C. Irvine, T. A. Moore, T. Jungwirth, and A. J. Ferguson, Phys. Rev. B **92**, 214406 (2015).